Evaluating the Mechanical Behavior of Arterial Tissue using Digital Image Correlation

by Dongsheng Zhang, Charles D. Eggleton and Dwayne D. Arola

ABSTRACT—In this study, digital image correlation (DIC) was adopted to examine the mechanical behavior of arterial tissue from bovine aorta. Rectangular sections comprised of the intimal and medial layers were excised from the descending aorta and loaded in displacement control uniaxial tension up to 40 percent elongation. Specimens of silicon rubber sheet were also prepared and served as a benchmark material in the application of DIC for the evaluation of large strains; the elastomer was loaded to 50 percent elongation. The arterial specimens exhibited a non-linear hyperelastic stress–strain response and the stiffness increased with percent elongation. Using a bilinear model to describe the uniaxial behavior, the average minor and major elastic modulii were 192±8 KPa and 912±40 KPa, respectively. Poisson's ratio of the arterial sections increased with the magnitude of axial strain; the average Poisson's ratio was 0.17±0.02. Although the correlation coefficient obtained from image correlation decreased with the percent elongation, a correlation coefficient greater than 0.8 was achieved for the tissue experiments and exceeded that obtained in the evaluation of the elastomer. Based on results from this study, DIC may serve as a valuable method for the determination of mechanical properties of arteries and other soft tissues.

KEY WORDS—Artery, digital image correlation (DIC), soft tissue

Introduction

The mechanical properties of arterial tissues contribute to our understanding of normal and pathological physiology, govern the design of prosthetic devices for the circulatory system, and help guide the development of non-invasive surgical techniques. Roy[1] was among the first to recognize the importance of arterial mechanics and constructed an apparatus to inflate arteries *in vitro* under known pressure. Compliance of the artery was calculated from the volume versus pressure curve. Pressure-diameter testing has remained a popular approach, but modern imaging techniques have been adopted to monitor changes in vessel geometry and volume that are associated with internal pressures.[2–4] Examples of other methods for measuring mechanical properties of arterial tissues include the use of photo cells combined with a scanning laser,[5] sono-micrometers,[6] differential transformers,[7] pasted wire strain gages,[8] and electrolytic transducers.[9] Many of the techniques employed for evaluating arterial mechanics have been reviewed by Hayashi.[10] Although these techniques have been applied both *in vitro* and *in vivo* they are either limited to small strains, require contact with the tissue, or can only measure strain in a single axis.

Non-contact methods are preferred for evaluating the mechanical properties of soft tissue because there is no change in stiffness resulting from the presence of a sensor. Imaging techniques are, therefore, very suitable candidates. Arterial tissues are hydrated, smooth, and generally devoid of distinguishing features that can be used as natural markers. However, displacements can be measured by applying artificial markers to the tissue in its relaxed state and monitoring the position of the markers during mechanical loading. For example, Zhou and Fung[11] and Humphrey *et al.*[12] introduced a four-point grid on the surface of tissue samples using a permanent ink marker to evaluate the non-linear elastic behavior of blood vessels. An inherent assumption in this approach is that the mechanical response is uniform and homogeneous between the marker points. Arterial tissue is composed of layers of elastin and collagen and there is a high degree of non-linearity in response to large strain.[13] Local variations in the anisotropy and inhomogeneity of arterial tissues have not been examined in detail, partly due to the limitations of most experimental techniques that have been adopted for analysis.

In the current study, digital image correlation (DIC) was adopted to determine the strain distribution in sections of bovine aorta subjected to uniaxial tension. The primary objective of this study was to evaluate the potential to use DIC for studying the mechanical behavior of soft tissue under a large range of strain, and to establish a suitable method for tissue preparation that is applicable for DIC. This analysis serves as an incremental step in using DIC to examine the mechanical behavior of soft tissues and in studying the effect of chemical and mechanical treatments on the change in properties of these materials.

Background

Digital image correlation is a non-contact optical method of displacement measurement that requires only two digital images for the evaluation of displacements. In contrast to point measurement techniques, DIC can provide the complete in-plane displacement distribution over a selected finite area of observation. The primary merits of DIC over other

Dongsheng Zhang is an Associate Research Scientist, Department of Mechanical Engineering, University of Maryland Baltimore County (also an Associate Professor, Department of Astronautical Technology, National University of Defense Technology, Changsha, People's Republic of China, 410073). Charles D. Eggleton and Dwayne D. Arola are Professors, Department of Mechanical Engineering, University of Maryland Baltimore County, Baltimore, MD 21250.

Original manuscript submitted: April 23, 2002.
Final manuscript received: August 7, 2002.

methods are that the optical arrangement is simple, either coherent or incoherent light can be used to illuminate the object's surface, and that the full-field deformation can be obtained over a large measurement range. For these reasons, DIC is viewed as a robust, flexible, and "easy to apply" measurement technique. It has been adopted to examine the deformation of structures,[14–16] mechanical behavior of engineering materials,[17–20] and plastic deformation of metals.[21,22]

Interaction between the incident light and the surface of an object results in a high contrast "speckle" image with random, high-frequency variation in light intensity. The distribution in light intensity $F(x, y)$ at each point and the surrounding neighborhood is unique. With deformation of the object, each position of the surface (x, y) is assumed to exist at a new location (x^*, y^*). The light intensity distribution at the new location should be consistent with the original distribution with only minor deviation. The in-plane surface displacement can be determined by finding the position of the light intensity distribution $F^*(x^*, y^*)$ which most closely resembles the original distribution $F(x, y)$. Digital images of the light intensity distribution can be acquired conveniently before and after deformation using a video camera or digital camera. The "speckle" distribution can then be represented by the grayscale intensity distribution. A search is performed to find the location on the deformed image with grayscale distribution that is most consistent with that on the original image representing the undeformed or reference state of the object. The surface displacements are then determined by comparing the positions of the grayscale distribution of the deformed image with respect to that of the original image.

The location of $F^*(x^*, y^*)$ can be obtained by calculating the correlation coefficient over the neighborhood of the deformed image and finding the position with the maximum correlation coefficient. The correlation coefficient (C) can be expressed as[18]

$$C = \frac{\langle FF^* \rangle - \langle F \rangle \langle F^* \rangle}{\left[\left\langle (F - \langle F \rangle)^2 \right\rangle \left\langle (F^* - \langle F^* \rangle)^2 \right\rangle \right]^{1/2}}, \tag{1}$$

where F and F^* are the grayscale matrices of the subset at position (x, y) in the undeformed image and (x^*, y^*) in the deformed image, respectively. The symbol $\langle\rangle$ in eq (1) implies the mean value of the elements in the matrix. Once the location with the maximum correlation coefficient is determined, the displacement between these two images can be determined according to

$$\begin{aligned} u &= x^* - x \\ v &= y^* - y. \end{aligned} \tag{2}$$

The corresponding engineering strain can be obtained from the first derivative of the displacements as

$$\begin{aligned} \varepsilon_x &= u_x = \frac{\mathrm{d}u}{\mathrm{d}x} \\ \varepsilon_y &= v_y = \frac{\mathrm{d}v}{\mathrm{d}y} \\ \gamma_{xy} &= \frac{1}{2}(u_y + v_x) = \frac{1}{2}\left(\frac{\mathrm{d}u}{\mathrm{d}y} + \frac{\mathrm{d}v}{\mathrm{d}x}\right). \end{aligned} \tag{3}$$

The in-plane Lagrangian strain components can also be obtained from the displacements ignoring out-of plane deformation according to

$$\begin{aligned} \varepsilon_x &= u_x + \frac{u_x^2 + v_x^2}{2} \\ \varepsilon_y &= v_y + \frac{u_y^2 + v_y^2}{2} \\ \gamma_{xy} &= \frac{u_y + v_x}{2} + \frac{u_x u_y + v_x v_y}{2}. \end{aligned} \tag{4}$$

The position of (x^*, y^*) may not lie an integer pixel distance from the original position. Therefore, interpolation of the grayscale between integer pixel locations is practiced in DIC to increase the accuracy of measurement. The most common methods of interpolation in DIC are bilinear and bicubic interpolations, and reports have indicated that bicubic is more accurate than bilinear.[23,24]

Materials and Methods

Specimen Preparation

The aorta and descending artery (total length from aortic arch of approximately 20 cm) were obtained within half an hour postmortem from two separate cows (Fig. 1(a)). The arteries were maintained in an ethylene glycol tetra-acetic acid (EGTA) enhanced passive physiologic solution except during transport, dissection, and testing. Each artery was cut axially between the thoracic ostia and laid flat, intimal side up. Several rectangular sections were excised from the descending portion of each aorta (Fig. 1(a)). The transverse and axial lengths were 20 mm and 100 mm, respectively. The adventitial and part of the medial layer of the specimens were removed using a microtome blade, yielding specimens comprised of the intimal and medial layers (Fig. 1(b)) with a uniform thickness of 2 mm. After sectioning, the specimens were flat with minimal curvature. Since the intimal surface is very smooth and wet, some unique procedures were required to generate random speckles on the surface to facilitate image correlation. The specimens were removed from the EGTA solution just prior to testing, and excess moisture was absorbed from the surface using paper cloth. A very thin coat of quick-drying black enamel (RUST-OLEUM) paint was sprayed onto the intimal surface using an aerosol can. The distance between the nozzle and specimen was maintained at 0.5 m, at least, to generate a fine mist of enamel that resulted in a uniform distribution of small paint dots. Using this simple procedure, a high-contrast speckle pattern was deposited on the specimen's surface, necessary for image correlation (Fig. 2(a)). Although the enamel paint contains solvents that may affect the properties of the tissue, the potential influence was ignored due to the small coating thickness and short period of testing time. In addition, the speckles were nearly dry on contact with the tissue, which further limited potential effects from the solvent.

To validate results obtained using DIC in evaluating properties of the bovine artery, benchmark tests were performed with a silicon rubber sheet (40 Durometer). Rectangular sections were obtained from the rubber sheet (1.6 mm thick) with dimensions of 25.4×85 mm^2. A speckle pattern was generated on the surface of the rubber specimens using the same spraying methods employed for the tissue.

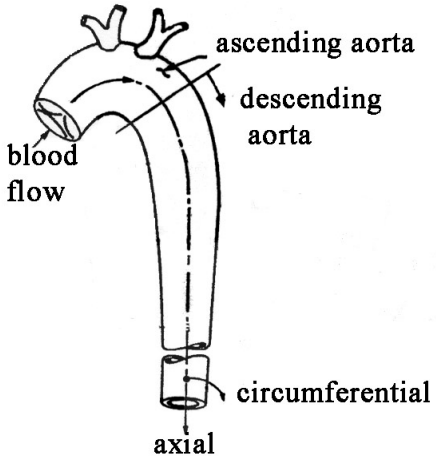

(a)

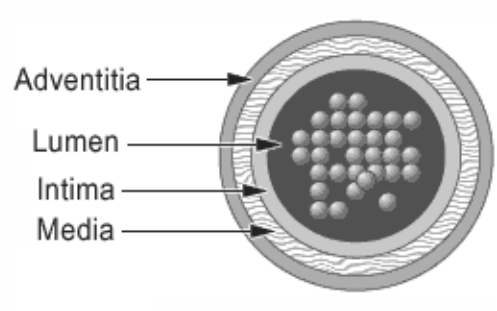

(b)

Fig. 1—Important features of the aorta and arterial tissue: (a) schematic diagram of the aorta and definition of the primary axes; (b) construction of the arterial wall

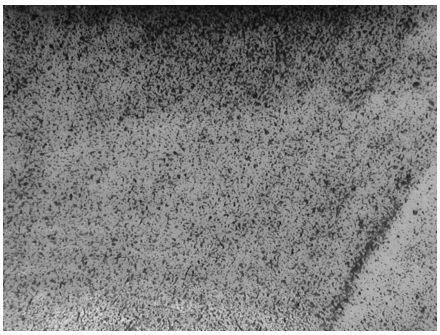

(a)

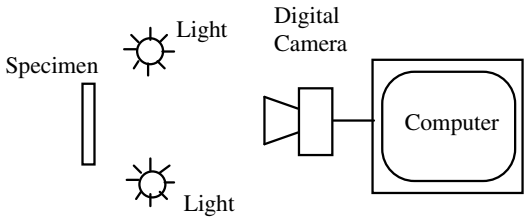

(b)

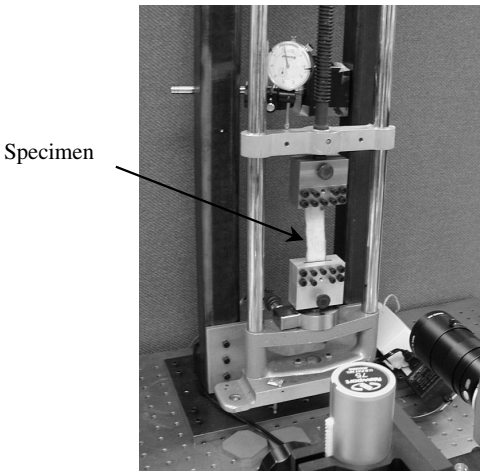

(c)

Fig. 2—Speckle pattern and optical arrangement for the experiments: (a) typical speckle field on the intimal surface resulting from the peripheral spray; (b) schematic diagram; (c) specimen mounted in the load frame

Loading Protocol

The specimens were placed within a dedicated load frame and subjected to uniaxial monotonic tensile loads under displacement control actuation. Compression grips were used to clamp both ends of the specimens; the gage lengths of the aorta and rubber specimens were 75 mm and 60 mm, respectively. Displacements were applied to the specimens along the axial direction in increments of 1.27 mm (0.05 in) through manual adjustment at an approximate strain rate of 1×10^{-3} s^{-1}. The arterial sections and rubber were subjected to a total axial deformation of 25 mm (1.0 in) and 33 mm (1.3 in), respectively. The resulting reaction load at each increment of elongation was determined using a Sensotec Model 41/0838 precision load cell with a full-scale range of 22.5 N and an accuracy of $\pm$ 0.2 percent. During the tensile test, the grip-to-grip displacement was monitored using a dial indicator. The indicated displacement was comprised of the uniform deformation of the arterial wall, restricted deformation near the compression grips, and sliding of the tissue within the grips at large strain. In general, the grip-to-grip strain was greater than the average strain computed using DIC at the central section. An image of the speckle pattern from the specimen's surface was recorded prior to loading and at each displacement increment. The elongation was kept constant for approximately 5 s while the digital image was captured at each increment. Speckle images were documented at every 2 percent elongation in the center of the gage section to avoid the influence of end effects; the axial load at each of these increments was also documented.

The tension experiments for the arterial specimens were comprised of loading the specimen to 25 percent elongation and unloading twelve times consecutively. The thirteenth and fourteenth cycles consisted of loading to 30 and 40 percent elongation and unloading, respectively. The first twelve cycles were conducted to condition the samples and achieve a steady-state mechanical response. Speckle images were documented during the first, fourth, eighth, twelfth, thirteenth, and fourteenth cycles at every 2 percent elongation; the axial

load at each of these increments was also documented. A typical experiment comprised of the fourteen load-unload cycles with one specimen required about 30 min. A bilinear model was used to describe the uniaxial response in which E_1 and E_2 represent the elastic modulus for small and large strains and are referred to as the minor and major elastic moduli, respectively. The minor elastic modulus was defined from a tangent line to the axial response up to 7 percent strain; the major modulus was estimated using the tangent approach for strains larger than 30 percent. Both the axial and transverse strains were available from the speckle images obtained at each increment of axial load. Thus, the Poisson ratio was determined as a function of the axial strain and load cycle for the arterial specimens. The silicon rubber specimens were subjected to displacement control uniaxial tension up to 50 percent elongation in increments of 2 percent and the speckle fields were documented at specific increments of the displacement. The minor elastic modulus was estimated using the tangent method up to 5 percent strain and the Poisson ratio of the rubber was estimated as a function of axial stretch up to 50 percent elongation. The mechanical behavior of the silicon rubber was also evaluated from uniaxial tension experiments conducted with an Instron Dynamite Model 8841 universal testing system. The system was equipped with a Model 75/C863 load cell with a maximum range of 1000 N. Experiments were conducted under displacement control actuation at a strain rate of 1×10^{-3} s^{-1}. The axial strain was monitored using an Epsilon Model 3442 miniature extensometer with 6 mm gage length and maximum elongation of 25 percent. The axial response was quantified in terms of the true stress and Lagrangian strain and then compared to the mechanical behavior found from experiments using DIC.

Optical Arrangement

The optical arrangement used in this study for DIC consisted of an Olympus Model C-3000Z digital camera with 7.5× zoom lens, an incoherent light source, and a desktop computer to acquire the digital images. The zoom lens was used to increase magnification of the digital image. The camera lens was located approximately 125 mm from the tissue surface, while the light source was 1m from the surface to minimize radiation heating. A schematic diagram of the experimental apparatus is shown in Fig. 2(b) and a picture of the specimen mounted within the load frame is shown in Fig. 2(c). An image size of 25×18 mm^2 was acquired using the camera and digitized into a sample of 1280×960 pixels with 256 gray levels. A comparison of the digitized speckle distributions captured at each load step was conducted to determine the full-field displacement distribution in the arterial and silicon rubber specimens.

Data Reduction

Digital image correlation was applied to analyze the strain distribution in the tissue and silicon rubber from the sequential images acquired during application of the axial loads. The first image taken without application of an axial load (zero load) represents that of the "undeformed object." In most circumstances, it is used as the reference image and is compared with those obtained after a particular magnitude of deformation to calculate the displacement and corresponding strain fields. However, to minimize speckle decorrelation, an interim speckle image obtained near the middle of the total elongation was used as the reference image and all displacements were determined with respect to this image. The intermediate reference image served as a non-zero offset with which all displacements and strains were calculated. As an alternative, an affine transformation could be used for large deformations with the use of modified elemental shape functions to further improve correlation.[25]

In this study a fast-search strategy was adopted to limit computational time while maximizing the precision of the displacement measurements;[26] the approach is a modification of the "coarse-fine" search strategy.[14] Initially, the search for the maximum correlation coefficient (C_{max}) is implemented at integer pixel locations until the location with the maximum correlation coefficient is found. An interpolation is not necessary during this search because the grayscale at subpixel locations is not needed. Near the integer pixel with C_{max}, the profile of the correlation coefficient must be smooth. As such, the gradient vector of the correlation coefficient can be found and used to guide the search directly towards the location with C_{max}. The benefit of this approach is to restrict interpolation and correlation calculations to those subpixel locations that lie on the path to C_{max}. The search step in the subpixel domain may be changed from 0.1 to 0.001 pixel length according to the required precision. The search with a search step of 0.1 pixels is conducted in an area of 2×2 pixels that is centered on the integer pixel with maximum correlation. When the subpixel location with C_{max} is found, the search is once again continued in the subpixel domain around the subpixel location with C_{max} identified in the previous step. The search step is then reduced to 0.01 pixels and the search domain is restrained to an area of 0.2×0.2 pixels and so on. All sub-pixel interpolation in this study was conducted using bi-cubic interpolation with a precision of 0.01 pixels.

Decorrelation of the speckle patterns may occur in the analysis of large deformations and can result in unreasonable errors. A reduction in correlation between the undeformed and deformed images will result in a decrease in the precision of displacement measurements obtained using DIC. The likelihood of decorrelation increases with the decrease in correlation coefficient. Therefore, the correlation coefficient obtained from the image correlation process was evaluated as a function of the elongation for the two materials examined in the experimental study. A simulated displacement field was also generated with known uniform strain to evaluate the precision of the fast search strategy algorithm. A typical speckle field resulting from preparation of an arterial section was used for the error analysis and the simulated strain was estimated using eq (3) over strains from 100 to 350×10^3 με. The correlation coefficient obtained over this range of strain analysis was greater than 0.6. However, the average error in the calculated strain field from DIC was within 1 percent of the simulated strain field. If the correlation coefficient decreased below 0.55, the calculated strain from the simulated displacement field showed an unacceptably large error.

The displacement fields within the arterial and silicon rubber resulting from uniaxial loading were used to calculate the corresponding strain distribution. The Lagrangian strain at any increment of elongation was obtained with respect to the unloaded condition using the calculated displacement gradients (eq (4)). Both the axial and transverse strain distributions were determined. The axial stress resulting from tensile loading at each increment of displacement was estimated from the load and cross-sectional area of the

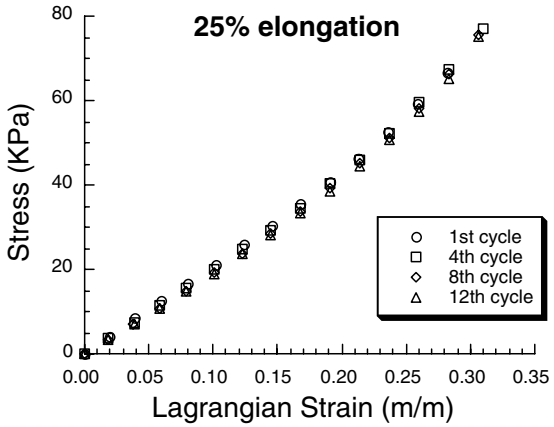

Fig. 3—Mechanical behavior of an arterial specimen under uniaxial tension during conditioning

specimens. The actual cross-sectional area at each state of deformation was obtained using the assumption that volume is preserved. Thus, the true stress in the specimen at each displacement increment was obtained from the initial gage length and incremental length obtained from the elongation.

Results

The arterial specimens were conditioned through twelve cycles of loading to 25 percent elongation and then unloaded, followed by loading to 30 and 40 percent elongation. A typical series of stress–strain curves obtained from an axial section during specific cycles of the conditioning routine is shown in Fig. 3. Using the tangent method with axial response to 7 percent strain, the estimated elastic modulus decreased from 212 KPa to 186 KPa from the first to the twelfth cycle. The results from the conditioning of axial specimens obtained from the two different animals are described in Table 1. For each tissue sample, the elastic modulus decreased with conditioning and reached a steady-state response near the tenth cycle. The axial response of a representative specimen during the thirteenth and fourteenth load cycle corresponding to 30 and 40 percent nominal elongation are shown in Figs. 4(a) and 4(b), respectively. As evident in all the stress–strain curves, the arteries exhibited non-linear behavior. When tested to 40 percent elongation, the constitutive behavior exhibited two characteristic regions including a region of low stiffness and a second region of higher relative stiffness. During conditioning, a reduction in the minor elastic modulus (E_1) occurred with repetition in the load cycle as expected. In addition, the modulus increased for cycles with larger axial stretch (cycles 13 and 14) as evident from Table 1. The major modulus (E_2) of the second component of the stress–strain curve in Fig. 4(b) was 884 KPa. The elastic constants for the two arteries at large strain are listed in Table 1. Although the samples were obtained from two different cows, the mechanical behavior of specimens was very similar.

The Poisson ratio was determined from the ratio of transverse and axial strains of each arterial section over the load history. Figure 5 shows the change in Poisson's ratio of a representative arterial specimen with elongation. A comparison of the mechanical response with each load cycle indicated that

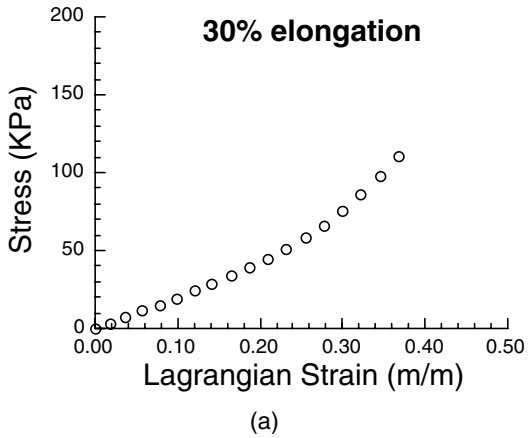

(a)

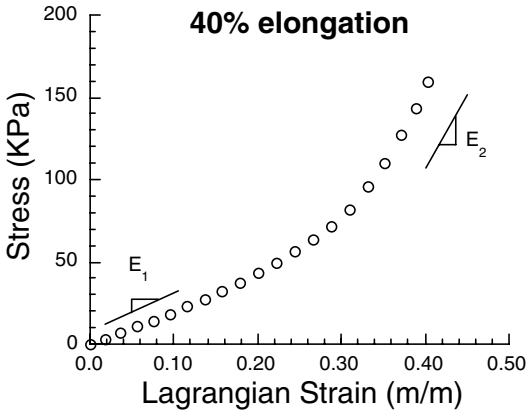

(b)

Fig. 4—Mechanical response of a specimen from Bovine 1 during uniaxial tension experiments: (a) 30 percent elongation; (b) 40 percent elongation

Poisson's ratio increased with the magnitude of axial stretch but decreased with each cycle of the conditioning phase of loading. However, with a change in the load cycle and an increase in the axial strain, the Poisson's ratio of each specimen increased. The change in response of the representative specimen for the fourteenth load cycle is apparent in Fig. 5; the average Poisson's ratio increased from 0.15 to about 0.23 and the overall average Poisson's ratio was 0.17 ± 0.02.

The true stress and Lagrangian strain for the silicon rubber were calculated at each displacement increment. A typical record of the stress–strain response is shown in Fig. 6(a). The results obtained using DIC are compared with the uniaxial response obtained using the universal test system and extensometer for displacement measurements in this figure. Note that the extensometer was removed prior to reaching its limit of 25 percent strain. The elastic modulus of the silicon rubber was determined using the tangent method and found to be 2.0 MPa for both methods of testing. Using the calculated transverse and axial strains from experiments with DIC, Poisson's ratio of the silicon rubber specimen was also determined as a function of the degree of elongation and is shown in Fig. 6(b). In contrast to the arterial response, Poisson's ratio of the elastomer decreased with elongation. The material behaved as an incompressible solid at the onset of deformation and then

TABLE 1—THE AVERAGE ELASTIC MODULUS OF ARTERIAL SPECIMENS FROM THE TWO BOVINE

	Bovine 1 Modulus		Bovine 2 Modulus	
Load Cycle	E_1 (KPa)	E_2 (KPa)	E_1 (KPa)	E_2 (KPa)
Cycle 1	212		192	
Cycle 4	193		190	
Cycle 8	187		184	
Cycle 12	186		183	
Cycle 13	194		190	
Cycle 14	195	884	193	940

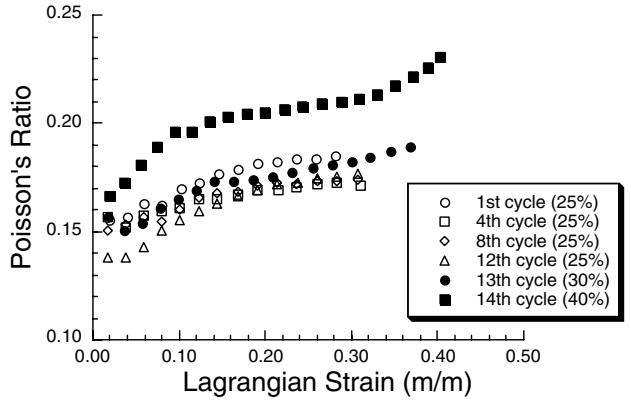

Fig. 5—Poisson's ratio of a specimen from Bovine 1 as a function of the percent elongation and load cycle. The average Poisson's ratio for all specimens and degree of axial stretch was 0.17±0.02

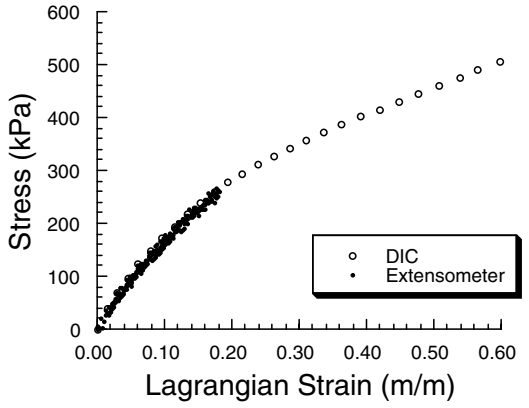

(a)

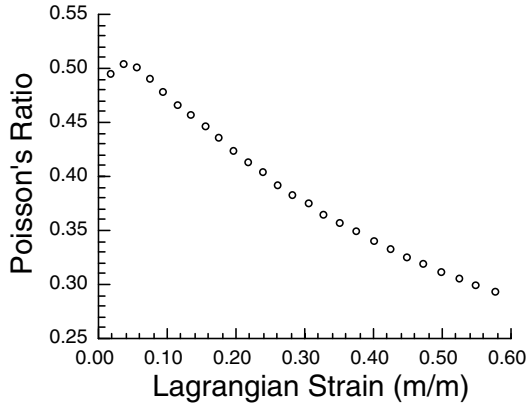

(b)

Fig. 6—Mechanical response of the silicon rubber from uniaxial tension experiments: (a) axial response of the rubber evaluated using displacement measurements from DIC and the extensometer; (b) change in Poisson's ratio with elongation

underwent significant volume change with an increase in axial strain. At the onset of deformation, the silicon rubber should behave as an incompressible solid and exhibit a Poisson's ratio of 0.5. In the first two increments of loading, the axial and transverse strains were small. Consequently, errors in the strain measurements would have the most influence on Poisson's ratio at small strains, as evident from Fig. 6(b). With an increase in strain, the contributions from errors in measurement decreased and the elastomer exhibited increasing compressibility as expected.

Discussion

A comparison of the stress–strain response of the bovine artery (Fig. 4) and silicon rubber (Fig. 6(a)) resulting from uniaxial loading reveals that the constitutive behavior of the two materials is characteristically quite different. Furthermore, the strain-dependent Poisson's ratio of the bovine artery and elastomer in Figs. 5 and 6(b), respectively, are also quite different. The Poisson's ratio of the arterial specimens increased with axial strain, while that of the elastomer decreased with axial strain. The elastomer exhibits incompressible behavior ($\nu = 0.5$) at the onset of loading and then becomes increasingly compressible with the extent of axial elongation. Note that additional experiments would be required to establish the characteristic response for each of the two materials in a more thorough manner.

Based on the trend in the Poisson's ratio of the elastomer in Fig. 6(b), it is apparent that there are some errors contributing to the experimental results, particularly at low strain ($\varepsilon \leq 8$ percent). To maintain conservation of volume, the Poisson's ratio of the elastomer should be less than or equal to 0.5; the calculated value obtained from the displacement field using DIC exceeded this quantity indicating a 2 percent error at least. The primary source of error in the experimental analysis results from out-of-plane displacement of the specimen during the onset of loading. This problem is especially troublesome in the testing of compliant materials. Out-of-plane displacement may cause defocusing and decorrelation of the speckles due to the perceived changes in speckle shape. Based on the optical arrangement and distance

from the camera to the specimen's surface, the maximum error associated with the out-of-plane displacement was less than 0.5 percent according to Sutton *et al.*[27] The load frame used for testing utilized swivel grips, which rely on the material's stiffness and/or axial load for self-alignment. An axial load can be applied to compliant materials to align the grips and minimize further out-of-plane displacement with increasing strain. However, if the specimen is subjected to an axial (offset) load to minimize the errors attributed to out-of-plane displacement, a component of axial and transverse strain exists within the specimen at the "apparent" unloaded state. The axial and transverse strains calculated at each increment of elongation beyond the unloaded state do not include the offset strains resulting from the pre-load. If the material is linearly elastic and Poisson's ratio is constant over this range there would be no error introduced by the pre-load. But the elastomer exhibits non-linear elastic behavior with a non-constant Poisson's ratio. Thus, the calculated Poisson's ratio for the elastomer has a component of error imposed by the offset load and is most prominent at small strains. The aforementioned sources of error are also present in the calculated strains for the arterial specimens due to the non-linear behavior and large compliance. However, the tissue's mechanical response to axial loading is also influenced by the residual stress existing within the intimal and medial layers.[28,29] The arterial specimens have a natural curvature in the circumferential direction resulting from the residual stress that can contribute to defocusing and speckle decorrelation as well. The effect of defocus on strain errors was not considered. Nevertheless, the constitutive behavior and elastic constants determined for the arterial specimens in this study agree with those reported in the literature. In addition, close agreement in the uniaxial response of the silicon rubber, characterized using the two methods of displacement measurement (Fig. 6(a)), provides validation to the experimental approach.

The elastic modulus reported for specimens comprised of intimal and medial layers of the descending aorta is 248 Kpa.[30] The mechanical properties of arteries are dominated by the medial layer as it is comprised of the highest percentage of collagen fibers. The specimens examined in this study were comprised of the intima and a portion of the media; the average elastic modulus after conditioning was 192 KPa. Based on the difference in ratio of intimal to medial components, it is reasonable that the elastic modulus was less than that reported in the literature. Note, however, that the axial stress was calculated using the actual cross-sectional area based on the assumption that volume is preserved. The distribution in Poisson's ratio in Fig. 5 indicates that volume was not preserved and that the actual cross-sectional area was greater than that used in calculating axial stress. Thus, the stress and corresponding elastic modulus would be smaller than those reported in Table 1.

It is generally assumed in the application of DIC that the grayscale distribution of the subset does not change appreciably with deformation. Changes in the grayscale distribution of a subset can cause the correlation coefficient to decrease. If the correlation coefficient decreases below a threshold value, decorrelation occurs and may result in large random errors. This problem often becomes more prominent with large deformation. Figure 7(a) shows the change in correlation coefficient with axial strain in the evaluation of the displacement fields of the arterial specimens. As evident from this figure the correlation coefficient decreased from 1.0 at the

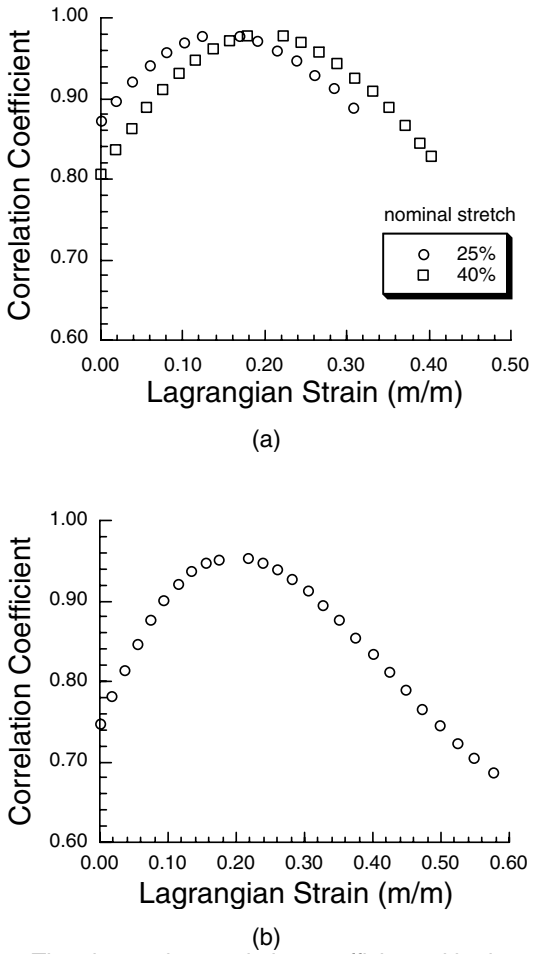

Fig. 7—The change in correlation coefficient with elongation of the test specimens. An arbitrary image was selected from near the middle of the total deformation and used as the reference in calculating the full-field strains (15 percent for 25 percent axial stretch and 20 percent for 40 and 50 percent axial stretch): (a) arterial specimen (Bovine 1); (b) silicon rubber specimen (benchmark loaded to 50 percent nominal elongation)

reference image to 0.8 at the largest degree of deformation. Similarly, Fig. 7(b) shows the change in correlation coefficient with axial strain for the benchmark experiments with silicon rubber. The correlation coefficient decreased from 1.0 to below 0.7 at the largest strain. A reference image was chosen near the middle of the total elongation for both materials and the correlation coefficient decreased with an increase in the absolute displacement with respect to this reference image. Consequently, the total decrease in correlation coefficient was reduced. If the unloaded specimen was used for reference, random errors due to decorrelation could become more prominent. This statement is especially true if the specimen in the unloaded state is not planar. Nevertheless, decorrelation was not a problem in examining deformation in the arterial specimens that resulted from uniaxial tension. Although the magnitude of the correlation coefficient does not indicate that the displacement and corresponding strains are accurate, it does increase confidence in the computed results.

Based on a comparison of the correlation coefficients resulting from an analysis of the tissue and silicon rubber in

Fig. 7, the image correlation process was not influenced by differences in elastic properties and surface hydration of the two materials. The correlation coefficients for the rubber and tissue are nearly identical at the same quantity of relative axial strain. Thus, the simple method of surface preparation used in this study is an effective way to generate speckle patterns that support the use of DIC. It is also relatively insensitive to whether the surface is wet or dry. The black speckle dots resulting from the peripheral paint spray easily attached to the wet surface and maintained shape during the axial loading. The deposited speckle pattern did not provide reinforcement to the specimens, which would contribute to the perceived constitutive behavior. Based on results from this study, DIC is an ideal experimental method of displacement measurement for the determination of mechanical properties of arteries and other soft tissues. Future experiments will be conducted using DIC to examine the anisotropy and structure dependent inhomogeneity of arterial tissues.

Conclusion

The mechanical behavior of the descending bovine aorta was examined under uniaxial tension. Digital image correlation (DIC) was adopted to document the in-plane surface displacements resulting from loading. A special, yet simplistic process was used to introduce a random high contrast speckle pattern onto the tissue surface. The specimens were conditioned from repeated loading to 25 percent elongation, and then loaded to 30 and 40 percent elongation. Additional experiments were conducted with a silicon rubber sheet for benchmarking results obtained using DIC under large strains (up to 50 percent).

1. The average minor elastic modulus (E_1) of the descending aorta from all load cycles was 192±8 KPa. The modulus decreased with each load cycle of conditioning and then increased with an increase in percent elongation. The average major elastic modulus (E_2) estimated from the axial response for strains greater than 30 percent was 912±40 KPa.

2. The Poisson's ratio of the aorta specimens increased with strain and each load cycle. At an axial elongation of 40 percent, the Poisson's ratio increased to 0.25. The average Poisson's ratio from all specimens and magnitude of axial strain was 0.17±0.02.

3. With proper surface preparation, DIC is a valid technique for examining the mechanical properties of hydrated soft tissue under a large range of deformation. The results from the experiments conducted with arterial specimens and silicon rubber indicate that DIC is capable of measuring in-plane strains up to 50 percent elongation without decorrelation.

References

1. Roy, C.S., "The Elastic Properties of the Artery Wall," J. Physiol., Lond., **3**, *125–162 (1881).*

2. Hayashi K., Takamizawa, K., Nakamura, T., and Tsushima, N., "Effects of Elastase on the Stiffness and Elastic Properties of Arterial Walls in Cholesterol Fed Rabbit," Atherosclerosis, **66**, *259–267 (1987).*

3. Weizsacker, H.W., and Pinto, J.G., "Isotropy and Anisotropy of the Arterial Wall," J. Biomech., **21**, *477–487 (1988).*

4. Carmines, D.V., McElhaney, J.H., and Stack, R., "A Piece-wise Nonlinear Elastic Expression of Human and Pig Coronary Arteries Tested in Vitro," J Biomech., **24**, *899–906 (1991).*

5. Papageorgiou, G.L., and Jones, N.B., "Circumferential and Longitudinal Viscoelasticity of the Human Iliac Arterial Segments in Vitro," J. Biomed. Eng., **10**, *82–90 (1988).*

6. Gentile, B.J., Chuong, C.J., and Ordway, G.A., "Regional Volume Distensibility of Canine Thoracic Aorta During Moderate Treadmill Exercise," Circ. Res., **63**, *1012–1019 (1988).*

7. Dorbin, P.B., "Biaxial Anisotropy of Dog Carotid Artery: Estimation of Circumferential Elastic Modulus," J. Biomech., **19**, *351–358 (1986).*

8. Gow, B.S., and Hadfield, C.D., "The Elasticity of Canine and Human Coronary Arteries with Reference to Postmortem Changes," Circ. Res., **45**, *588–594 (1979).*

9. Michelini, L.C., and Krieger, E.M., "Aortic Caliber Changes During Development of Hypertension in Freely Moving Rats," Am. J. Physiol., **250**, *H662–H671 (1986).*

10. Hayashi, K., "Experimental Approaches on Measuring the Mechanical Properties and Constitutive Laws of Arterial Walls," ASME J. Biomech. Eng., **115**, *481–488 (1993).*

11. Zhou, J., and Fung, Y.C., "The Degree of Nonlinearity and Anisotropy of Blood Vessel Elasticity," Proc. Natl. Acad. Sci., **94**, *14255–14260 (1997).*

12. Humphrey, J.D., Vawter, D.L., and Vito, R.P., "Quantification of Strains in Biaxially Tested Soft Tissues," J. Biomech., **20**, *59–65 (1987).*

13. Silver, F.H., Christiansen, D.L., and Buntin, C.M., "Mechanical Properties of the Aorta: A Review," Crit. Rev. Biomed. Eng., **17**, *323–358 (1989).*

14. Chu, T.C., Ranson, W.F., Sutton, M.A., and Peters, W.H., "Applications of Digital-Image-Correlation Techniques to Experimental Mechanics," EXPERIMENTAL MECHANICS, **25**, *232–244 (1985).*

15. Sutton, M.A., Chao, Y.-J., and Lyons, J.S., "Computer Vision Methods for Surface Deformation Measurements in Fracture Mechanics, Novel Experimental Techniques in Fracture Mechanics," ASME-AMD 176, 203–217 (1993).

16. Lu, H., Vendroux, G., and Knauss, W.G., "Surface Deformation Measurements of a Cylindrical Specimen by Digital Image Correlation," EXPERIMENTAL MECHANICS, **37**, *433–439 (1997).*

17. Zhao, W., and Jin, G., "An Experimental Study on Measurement of Poisson's Ratio with Digital Correlation Method," J. Appl. Polym. Sci., **60**, *1083–1088 (1996).*

18. Zhang, D., Zhang, X., and Cheng, G., "Compression Strain Measurement by Digital Speckle Correlation," EXPERIMENTAL MECHANICS, **39**, *62–65 (1999).*

19. Bastawros, A.-F., Bart-Smith, H., and Evans, A.G., "Experimental Analysis of Deformation Mechanisms in Closed Cell Aluminum Alloy Foam," J. Mech. Phys. Solids, **48**, *301–322 (2000).*

20. McGowan, D.M., Ambur, D.R., Hanna, T.G., and McNeill, S.R., "Evaluating the Compressive Response of Notched Composite Panels Using Full-field Displacements," J. Aircraft, **38**, *122–129 (2001).*

21. Tong, W., "Detection of Plastic Deformation Patterns in a Binary Aluminum Alloy," EXPERIMENTAL MECHANICS, **37**, *452–459 (1997).*

22. Wattrisse, B., Chrysochoos, A., Muracciole, J.-M., and Nemoz-Gaillard, M., "Analysis of Strain Localization During Tensile Tests by Digital Image Correlation," EXPERIMENTAL MECHANICS, **41**, *29–39 (2001).*

23. Bruck, H.A., McNeill, S.R., Sutton, M.A., and Peter, W.H., "Digital Image Correlation Using Newton-Raphson Method of Partial Differential Correction," EXPERIMENTAL MECHANICS, **29**, *261–267 (1989).*

24. Schreier, H.W., Braasch, J.R., and Sutton, M.A., "Systematic Errors in Digital Image Correlation Caused by Intensity Interpolation," Opt. Eng., **39**, *2915–2921 (2000).*

25. www.correlatedsolutions.com/videoextensometer/

26. Zhang, D., and Arola, D., "A New Fast-search Strategy for Digital Image Correlation," Proc. SEM Annual Conference on Theoretical, Experimental and Computational Mechanics, Milwaukee, Wisconsin, June 10-12, 2001, Paper No. 80.

27. Sutton, M.A., Chae, T.L., et al.*, "Development of a Computer Vision Methodology for the Analysis of Surface Deformations in Magnified Images," ASTM STP-1094, MICON-90, 109–132 (1990).*

28. Taber, L.A., and Humphrey, J.D., "Stress Modulated Growth, Residual Stress, and Vascular Heterogeneity," ASME J. Biomech. Eng., **123**, *528–535 (2001).*

29. Greenwald, S.E., Moore, J.E., Rachev, A., Kane, T.P.C., and Meister, J.-J., "Experimental Investigation of the Distribution of Residual Strains in the Artery Wall," ASME J. Biomech. Eng., **119**, *438–444 (1997).*

30. Fung Y.C., "Biomechanics. Mechanical Properties of Living Tissues," 2nd edn, Springer, 1993.